Korean J. Electron Microscopy Special Issue 1, 63~69(2006)

Electron Holography of Advanced Nanomaterials

D. Shindo*, H.S. Park, J.J. Kim, T. Oikawa[1] and T. Tomita[1]
Institute of Multidisciplinary Research for Advanced Materials, Tohoku University,
1-1 Katahira, 2-Chome, Aobaku, Sendai, 980-8577, Japan
[1]JEOL Ltd., 1-2 Musashino, 3-Chome, Akishima, Tokyo, 196-8558, Japan
(Received May 23, 2005; Accepted March 24, 2006)

ABSTRACT

By utilizing a field emission gun and a biprism installed on a transmission electron microscope (TEM), electron holography is extensively carried out to visualize the electric and magnetic fields of nanomaterials. In the electric field analysis, the distribution of electric potential in a sharp tip made of W coated with ZrO_2 is visualized by applying the voltage to the tip. Denser contour lines due to the electric potential are observed with an increase in the bias voltage. In the magnetic field analysis by producing the strong magnetic field with a sharp magnetic needle made of a permanent magnet, the *in situ* experiment is carried out to investigate the magnetization of hard magnetic materials. The results of these experiments clearly demonstrate that electron holography is a promising advanced transmission electron microscopy technique to characterize the electric and magnetic properties of nanomaterials.

Key words : Electric field, Electron holography, Magnetic field, Nanomaterials

INTRODUCTION

So far, high-resolution electron microscopy (Cowley, 1981; Spence, 1981; Shindo & Hiraga, 1998) and analytical electron microscopy (Reimer, 1993; Williams & Carter, 1996; Shindo & Oikawa, 2002) have been extensively carried out in order to characterize nanomaterials. While the resolution limit of TEMs reaches 0.1 nm, the probe size of incident electron beam comes down to less than 1 nm. With such a small probe, energy dispersive X-ray spectroscopy (EDS) and electron energy-loss spectroscopy (EELS) have been carried out at a nanometer scale. Thus, analytical techniques for microstructure, composition and electronic structure have been established and applied to various advanced materials. Recently, by utilizing a highly coherent electron beam produced by a cold or thermal field emission gun (FEG), electron holography experiments have been widely carried out. Among various electron microscopy techniques, electron holography provides a unique method for detecting the phase shift of the electron wave due to the electric and magnetic fields (Sindo & Oikaga, 2002; Tonomura, 1999; Volkl et al., 1999). Thus, it is expected that the electric and magnetic properties of various nanomaterials can be characterized by this technique. Actually, some of the present authors have carried out electron holography on various nanomaterials. As electric field analysis, the mean inner potential of SiO_2 particles has been quantitatively evaluated (Lee et al., 2002), and their charging effect has been analyzed through computer simulation (Aoyama et al., 2002). On the other hand, in the magnetic field analysis, the domain structures of nanocrystalline soft magnetic materials, i.e., $Fe_{73.5}Cu_1Nb_3Si_{13.5}B_9$ (Shindo et al., 2002) and Co-Zr-O (Liu et al., 2003) have been analyzed in detail. Also, the magnetic phase transformation of a hole-doped manganite $La_{0.81}Sr_{0.19}MnO_3$ has recently been observed (Murakami et al., 2003). In this paper, electron holography is carried out *in situ* to investigate

* Correspondence should be addressed to Dr. D. Shindo, Institute of Multidisciplinary Research for Advanced Materials, Tohoku University, 1-1 Katahira, 2-Chome, Aobaku, Sendai, 980-8577, Japan.

the electric field and magnetic field of nanomaterials by applying the voltage and magnetic field to them. A specially arranged specimen holder (Sindo et al., 2004), in which the sharp tip can be moved three-dimensionally using a stepping motor and piezo drives, has been effectively utilized for *in situ* experiments with applying the voltage and magnetic field.

MATERIALS AND METHODS

1. Experimental procedure

Electron holography experiment was carried out with a JEM-3000F TEM installed with a thermal FEG and a biprism. In a conventional TEM, magnetic domain structures are broken or modified due to a strong magnetic field of the objective lens. To overcome the difficulty, a special objective lens for magnetic domain observation has been introduced (Sindo et al., 2003). A spherical aberration coefficient (C_s) of an objective lens is 165 mm. When the objective lens is turned on, a spacing of the interference fringes is about 2.4 nm at a biprism voltage of 50 V, and the magnetic field of the objective lens at the specimen position is estimated to be about 1600 A/m. The spatial resolution and width of field of view are 7.2 nm and 460 nm, respectively. When the objective lens is turned off, a spacing of the interference fringes is about 25 nm at a biprism voltage of 40 V, and the magnetic field is estimated to be about 160 A/m. The spatial resolution and width of field of view are 75 nm and 3,000 nm, respectively.

To perform *in situ* observations of the electric field and magnetic field of nanomaterials, a specimen holder, where sharp tips made of W coated with ZrO_2 (W-ZrO_2 tip) and $Nd_2Fe_{14}B$ can be set as shown in Fig. 1(a), has been used. The W-ZrO_2 tip is commercially available as an electron source for a transmission electron microscope. The magnetic needle was made by a two-step electropolishing process (Sindo et al., 2004). The magnetic properties of the specimens investigated in this

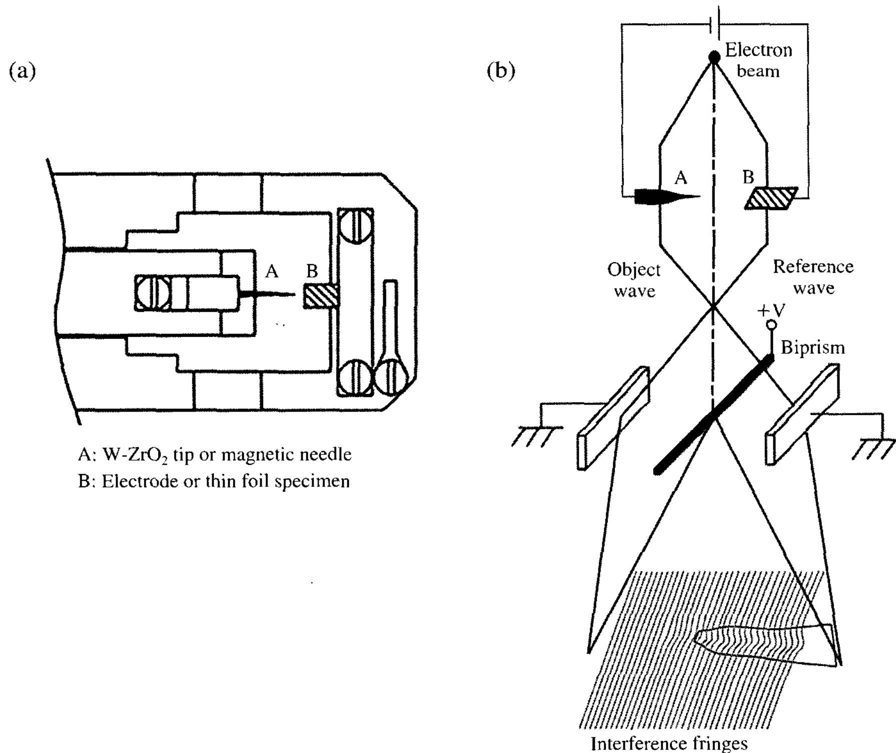

Fig. 1. (a) Schematic illustration of a part of a specimen holder equipped with a sharp tip. (b) Schematic illustration of hologram formation in a TEM.

Table 1. Magnetic properties of sintered $Nd_2Fe_{14}B$ and nanocomposite $Nd_{4.5}Fe_{77}B_{18.5}$

Specimen	Coercivity H_c (kA/m)	Remanence B_r (T)	Energy product $(BH)_{max}$ (kJ/m^3)
Sintered $Nd_2Fe_{14}B$	1,100	1.39	368
Nanocomposite $Nd_{4.5}Fe_{77}B_{18.5}$	248	1.03	58

study are presented in Table 1.

2. Imaging process of electron holography

In this section, the imaging process of electron holography on the basis of the digital data analysis is outlined. Electron holography is carried out through the two-step imaging process. In the first step, a hologram is formed using a biprism by which an object wave passing through a specimen interferes with a reference wave passing through the vacuum. In the second step, the phase shift of the electron wave is extracted from the hologram using Fourier transform.

Figure 1(b) shows a schematic illustration of hologram formation in a TEM. An electron beam emitted from a field emission tip is accelerated and then collimated to illuminate an object through a condenser lens system. An object is located in one half of the object plane that is illuminated by a collimated electron beam. Assuming that the object is illuminated by a plane wave of a unit amplitude having a wave vector parallel to the optical axis, the change of the scattering amplitude of the plane wave due to the object, in general, is described as

$$q(\boldsymbol{r})=A(\boldsymbol{r})\exp(i\phi(\boldsymbol{r})) \tag{1}$$

where $A(\boldsymbol{r})$ and $\phi(\boldsymbol{r})$ are real functions and describe the amplitude change and the phase shift due to the object, res-pectively. Since specimens are usually thin films, in most cases the vector $\boldsymbol{r}$ is confined to the film plane. Due to the use of the biprism, the object wave and the reference wave are tilted by $-\frac{\alpha_h}{2}$ and $\frac{\alpha_h}{2}$, respectively. Thus, the intensity of the hologram is given by

$$\begin{aligned} I_h(\boldsymbol{r})&=\left|A(\boldsymbol{r})\exp\left[-\pi i\frac{\alpha_h}{\lambda}x+i\phi(\boldsymbol{r})\right]+\exp\left[\pi i\frac{\alpha_h}{\lambda}x\right]\right|^2 \\ &=1+A^2(\boldsymbol{r})+2A(\boldsymbol{r})\cos\left(2\pi\frac{\alpha_h}{\lambda}x-\phi(\boldsymbol{r})\right) \end{aligned} \tag{2}$$

By performing a Fourier transform (F) of the hologram, one can obtain

$$\begin{aligned} F[I_h(\boldsymbol{r})]=&\delta(u)+F[A^2(\boldsymbol{r})] \\ &+F[A(\boldsymbol{r})\exp(i\phi(\boldsymbol{r}))]*\delta\left[u+\frac{\alpha_h}{\lambda}\right] \\ &+F[A(\boldsymbol{r})\exp(-i\phi(\boldsymbol{r}))]*\delta\left[u-\frac{\alpha_h}{\lambda}\right] \end{aligned} \tag{3}$$

(*: Convolution operation)

where the first and second terms are called "autocorrelation," while the other two terms are called "sidebands." By selecting the third term, shifting it by $\frac{\alpha_h}{\lambda}$, and performing an inverse Fourier transform (F^{-1}) on this term, we can obtain the phase shift and the amplitude change of the reconstructed image as digital data. In the following discussion, the intensity of the reconstructed phase image $I_{ph}(\boldsymbol{r})$ is represented by a cosine function, i.e.,

$$I_{ph}(\boldsymbol{r})=\cos(\phi(\boldsymbol{r})) \tag{4}$$

If necessary, the amplification of the phase can be calculated by multiplying the phase $\phi(\boldsymbol{r})$ by an integer n. It is noted that the radius of the region (sideband) selected is usually set to be $(1/3)\left(\frac{\alpha_h}{\lambda}\right)$.

Generally, the phase shift $\phi(\boldsymbol{r})$ is contributed from the electric potential φ and the magnetic flux Φ. The relation between the phase shift ϕ and the electrical potential φ is given as

$$\phi(\boldsymbol{r})=\sigma\int\varphi(x,y,z)\,dz,\ \left(\sigma=\frac{2\pi}{\lambda V(1+\sqrt{1-\beta^2})},\ \beta=v/c\right) \tag{5}$$

where v, c, and σ are the electron velocity, the light velocity, and the interaction constants depending on the accelerating voltage of the electron microscope (V) and the electron wavelength (λ). On the other hand, the relation between the phase shift ϕ and the magnetic flux density (and the magnetic flux) is given by

$$\phi(\boldsymbol{r})=\frac{2\pi e}{h}\oint\mathbf{A}ds=\frac{2\pi e}{h}\iint\mathbf{B}_n dS=\frac{2\pi e}{h}\Phi \tag{6}$$

where e, h, and $\boldsymbol{A}$ represent the elementary electric charge, Planck's constant, and the vector potential, respectively. Further, $\boldsymbol{B}_n$ and Φ correspond to the in-plane component of magnetic flux density and magnetic flux, respectively, and they are perpendicular to the incident

electron beam. It is noted that the sign of the phase shift changes depending on the direction of the magnetic flux.

RESULTS AND DISCUSSION

1. Analysis of electric field

Taking a W-ZrO_2 tip, the electric potential distribution around the tip is investigated by electron holography by applying the voltage. Figures 2(a) and (b) show a TEM image and an electron hologram of the W-ZrO_2 tip, respectively. The top of the tip is observed as a flat surface of the W (100) plane. Figures 2(c)-(f) show the reconstructed phase images of the W-ZrO_2 tip with different bias voltages applied. It is clearly seen that the contour lines due to the electric potential are visualized, and they have a symmetrical distribution around the W-ZrO_2 tip. With an increase in the bias voltage, the number of contour lines increases while the distance between the contour lines decreases. These results indicate that the strength of electric field becomes larger around the W-ZrO_2 tip, caused by the bias voltage applied. Also, it is reasonably considered that a phenomenon of field electron emission by applying the voltage can be induced preferentially at the region where the distance between contour lines is the shortest, i.e., the region with the strongest electric field.

2. Analysis of magnetic field

Magnetic microstructure is another important target in electron holography studies. Particularly, by changing the applied magnetic field, we can perform *in situ* observations regarding the magnetization process, from which essential information of the magnetic properties is obtained. Here we report our recent observations about the effects of the applied magnetic field to the hard magnetic materials.

Although electron holography is an useful technique to analyze *in situ* the magnetization process, the magnetic field applied in the thin film plane is so limited due to the deflection of the incident electron beam. Here, in order to observe the magnetization process of especially hard magnetic materials, a sharp needle made of sintered $Nd_2Fe_{14}B$, which may generate a fairly strong magnetic field, is prepared and used for magne-

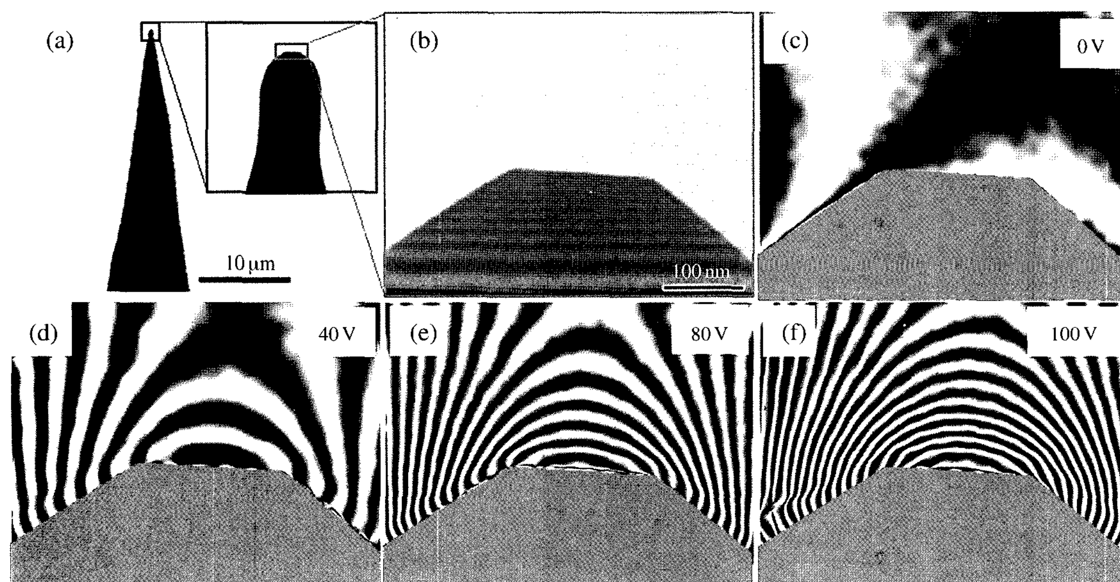

Fig. 2. (a) TEM image of a W-ZrO_2 tip. (b) Electron hologram of a W-ZrO_2 tip obtained when the bias voltage is V=100 V. (c)-(f) Reconstructed phase images of a W-ZrO_2 tip obtained when the bias voltages are V=0, 40, 80, and 100 V, respectively. The distance between the W-ZrO_2 tip and the electrode is 2 μm. The phase is amplified by 3.

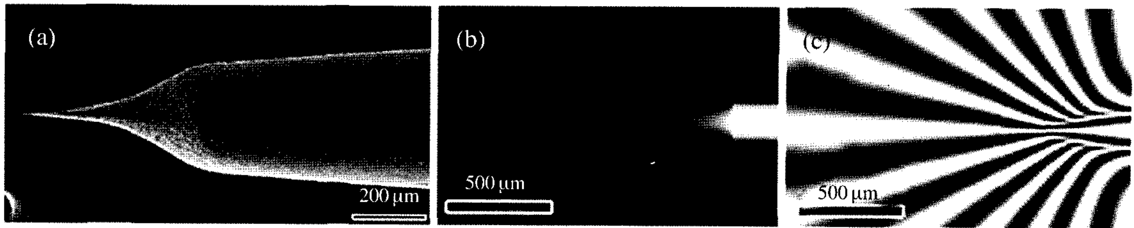

Fig. 3. (a) SEM image of the sharp magnetic needle. (b) Simulation of the magnetic needle. (c) Simulated image showing the magnetic field distribution.

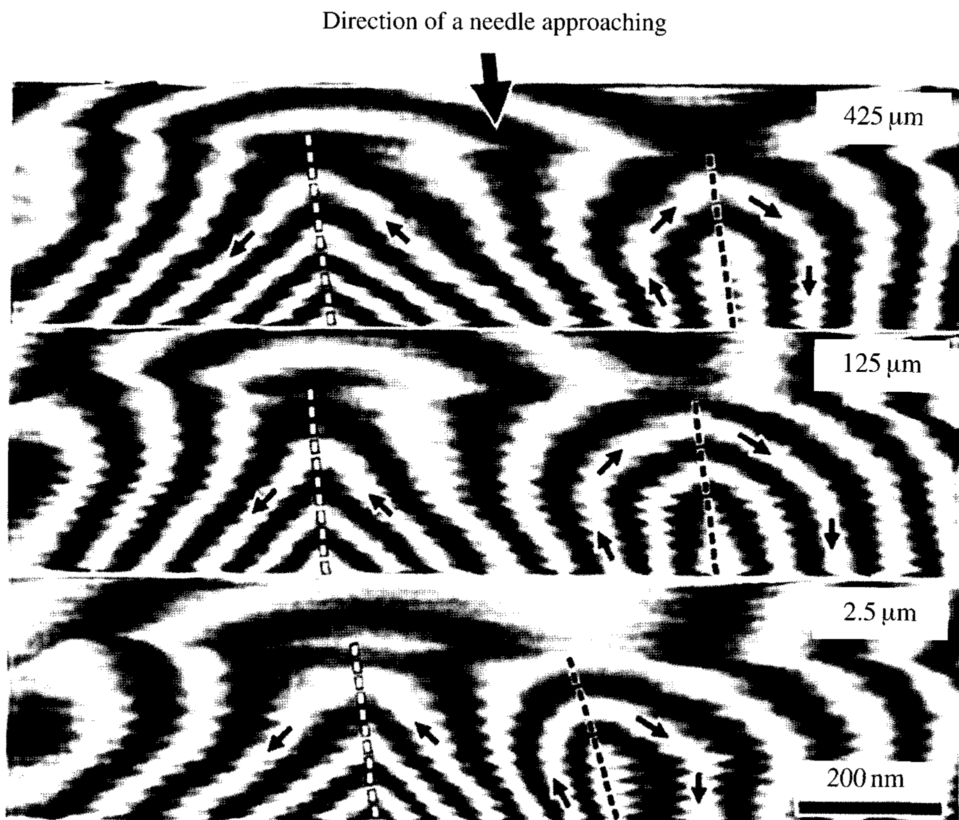

Fig. 4. Reconstructed phase images of sintered $Nd_2Fe_{14}B$ with the needle approaching. The phase is amplified by 2. The distance between the needle and the specimen is shown in each figure. The directions of the needle approaching are indicated with a big arrow at the top.

tization experiment. Thus, electron holography is carried out utilizing this magnetic needle to investigate the magnetization process of hard magnetic materials at a nanometer scale.

Figure 3(a) shows a SEM image of the sharp magnetic needle made of sintered $Nd_2Fe_{14}B$. When a magnetic field of 1.0 T was applied to the magnetic needle by an electromagnet, the remanence of the sharp needle was estimated to be approximately 0.9 T. Figures 3(b) and (c) show the simulations of the magnetic needle and

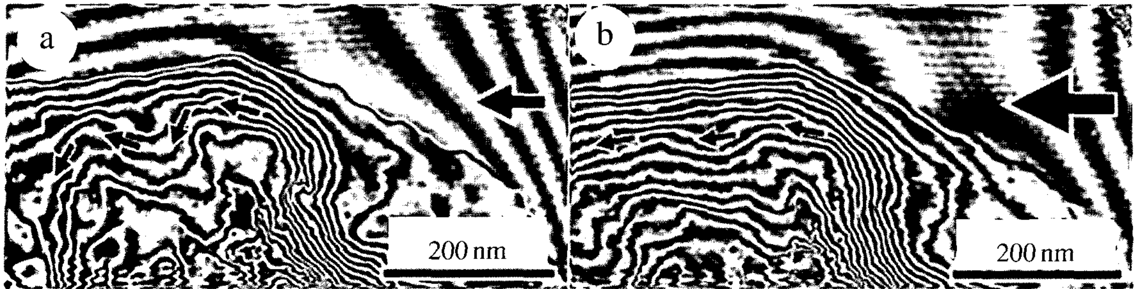

Fig. 5. Reconstructed phase images of nanocomposite $Nd_{4.5}Fe_{77}B_{18.5}$ annealed at 983°K. The distance between the needle and the specimen in (b) is smaller than in (a). Small arrows indicate the direction of lines of magnetic flux, while the big arrow indicates the direction of the needle approaching. The phase is amplified by 5.

reconstructed phase image showing the magnetic field distribution. By assuming the remanence of the sharp needle to be approximately 0.9 T, the magnetic flux density at the top of the needle is estimated to around 0.7 T through the simulation.

Figure 4 shows reconstructed phase images of a sintered $Nd_2Fe_{14}B$ specimen, which is known as a typical *nucleation-type permanent magnet*. In Fig. 4, both the specimen and the needle are demagnetized $Nd_2Fe_{14}B$. The distance between the needle and the specimen is indicated at the top right of each figure. The white bands or black bands correspond to the distribution of lines of magnetic flux, whose direction is indicated by the arrows. The domain walls indicated by dotted lines shift gradually when the needle comes close to the specimen. It can be interpreted that the magnetic field applied acts as a pressure perpendicular to the parallel domain walls. From the figures, it is observed that the area of domains magnetized parallel to the direction of the needle approaching increases, while that of the domains magnetized in the antiparallel direction gradually decreases. It is seen that the magnetic domain walls can be shifted easily from the demagnetized state.

Strong magnetic field produced by the sharp magnetic needle was also applied to nanocomposite $Nd_{4.5}Fe_{77}B_{18.5}$. Figures 5(a) and (b) are reconstructed phase images showing the magnetization process from the demagnetized state of nanocomposite $Nd_{4.5}Fe_{77}B_{18.5}$ annealed at 983°K. A magnetic field (2.5 T) was applied to the needle by an electromagnet. When the distance between the needle and the specimen is large, the distribution of lines of magnetic flux forming a closure domain does not change so much as shown in Fig. 5(a). On the other hand, when the needle comes close to the specimen in Fig. 5(b), the direction of lines of magnetic flux tends to be parallel to the magnetic field generated by the needle, showing the gradual magnetization process of nanocomposite $Nd_{4.5}Fe_{77}B_{18.5}$. Thus, it is demonstrated that electron holography with a sharp magnetic needle is quite useful to investigate the magnetization process of nanocomposite magnets.

CONCLUSIONS

Electron holography was carried out *in situ* by applying the voltage and magnetic field to nanomaterials. In the $W\text{-}ZrO_2$ tip, the change of distribution of electric potential with an increase in the bias voltage between the $W\text{-}ZrO_2$ tip and the electrode was clarified. On the other hand, the strong localized magnetic field was produced through a sharp magnetic needle made of a permanent magnet set in the specially designed specimen holder, and the strong magnetic field was utilized to investigate the magnetization process of hard magnetic materials by electron holography. Electron holography with the use of nanotips as demonstrated here is promising to investigate the electric and magnetic properties of various advanced nanomaterials.

REFERENCES

Cowley JM: Diffraction Physics 2nd Ed. North-Holland,

Amsterdam, 1981.
Spence JCH: Experimental High-Resolution Electron Microscopy Clarendon Press, Oxford, 1981.
Shindo D, Hiraga K: High-Resolution Electron Microscopy for Materials Science Springer-Verlag, Tokyo, 1998.
Reimer L: Transmission Electron Microscopy 3rd Ed. Springer-Verlag, Berlin Heidelberg, 1993.
Williams DB, Carter CB: Transmission Electron Microscopy IV Plenum Press, New York, 1996.
Shindo D, Oikawa T: Analytical Electron Microscopy for Materials Science Springer-Verlag, Tokyo, 2002.
Tonomura A: Electron Holography 2nd Ed. Springer-Verlag, Tokyo, pp. 78-116, 1999.
Volkl E, Allard LF, Joy DC: Introduction to Electron Holography Kluwer Academic/Plenum Publishers, New York, 1999.
Lee CW, Ikematsu Y, Shindo D: J Electron Microsc 51 : 143, 2002.
Aoyama Y, Park YG, Lee CW, Shindo D: JIM 43 : 474, 2002.
Shindo D, Park YG, Yoshizawa Y: J Magn Magn Mater 238 : 101, 2002.
Liu Z, Shindo D, Onuma S, Fujimori H: J Magn Magn Mater 262 : 308, 2003.
Murakami Y, Yoo JH, Shindo D, Atou T, Kikuchi M: Nature 423 : 965, 2003.
Shindo D, Park YG, Gao Y, Park HS: J Appl Phys 95 : 6521, 2004.
Shindo D, Park YG, Murakami Y, Gao Y, Kanekiyo H, Hirosawa S: Script Mater 48 : 851, 2003.